

# Rothamsted Repository Download

## A - Papers appearing in refereed journals

Van der Vaart, K., Sinhuber, M., Reynolds, A. M. and Ouellette, N.T.  
2019. Mechanical spectroscopy of insect swarms. *Science Advances*. 5  
(7), p. eaaw9305.

The publisher's version can be accessed at:

- <https://dx.doi.org/10.1126/sciadv.aaw9305>

The output can be accessed at:

<https://repository.rothamsted.ac.uk/item/8wqy4/mechanical-spectroscopy-of-insect-swarms>.

© 10 July 2019, Please contact [library@rothamsted.ac.uk](mailto:library@rothamsted.ac.uk) for copyright queries.

## ECOLOGY

## Mechanical spectroscopy of insect swarms

Kasper van der Vaart<sup>1</sup>, Michael Sinhuber<sup>1</sup>, Andrew M. Reynolds<sup>2</sup>, Nicholas T. Ouellette<sup>1\*</sup>

Social animals routinely form groups, which are thought to display emergent, collective behavior. This hypothesis suggests that animal groups should have properties at the group scale that are not directly linked to the individuals, much as bulk materials have properties distinct from those of their constituent atoms. Materials are often probed by measuring their response to controlled perturbations, but these experiments are difficult to conduct on animal groups, particularly in the wild. Here, we show that laboratory midge swarms have emergent continuum mechanical properties, displaying a collective viscoelastic response to applied oscillatory visual stimuli that allows us to extract storage and loss moduli for the swarm. We find that the swarms strongly damp perturbations, both viscously and inertially. Thus, unlike bird flocks, which appear to use collective behavior to promote lossless information flow through the group, our results suggest that midge swarms use it to stabilize themselves against environmental perturbations.

## INTRODUCTION

Acting collectively is widely thought to endow animal groups with a range of benefits (1–3). Groups are, for example, thought to be better able to sense and respond to stochastic and uncertain environments than individuals (4). They may exploit collectivity to migrate (5, 6), forage (7), and build (8, 9) more efficiently. And the much-vaunted “wisdom of the crowd” effect suggests that groups as a whole are more knowledgeable than any single individual (10). There are thus substantial incentives for understanding what group-level effects are possible and how and why they arise, both to deepen our general understanding of complex interacting systems and to exploit collectivity in engineered systems (11, 12). These goals can be addressed by building models, often grounded in statistical physics (3, 13, 14).

These models typically posit a set of individual-level interactions that when scaled up produce group structure and function. Observationally, however, one can only measure the outcome of any such interaction rules—and since many different interactions can lead to very similar group-level behavior (1), trying to recover the rules to validate models requires the solution of a difficult, and likely ill-posed, inverse problem (15). Instead, we here work at the group level and directly consider the emergent properties of the aggregation. Rather than passively observing only the group pattern and morphology, however, which contain little precise information (1), we take inspiration from materials testing and characterize the group response to a controlled applied stimulus (16–18). This approach allows us to extract emergent group properties that are not directly linked to the characteristics of the individuals (16, 19), much as bulk materials have well-defined properties that are distinct from those of their constituent atoms.

Here, we show that at a macroscopic level, when driven by an oscillatory visual cue, swarms of the nonbiting midge *Chironomus riparius* respond as if they are viscoelastic. More particularly, comparing the effective storage and loss moduli of the swarm, we find that the swarms are dominated by viscous and inertial damping. We also show that these results are reproduced by a simple stochastic model for the swarm where the visual system of the midges is not explicitly described. Our results suggest that collective behavior in midge swarms serves to provide stability and robustness against environmental perturbations,

consistent with their biological function and in contrast to other collective systems such as bird flocks and fish schools.

## RESULTS

## Controlled dynamic stimuli for midge swarms

Providing controlled stimuli to an animal group like a swarm is more challenging than for a normal material (16, 18, 20). One way to do so would be to confine the group in a container and apply a true mechanical stress (16). Such an experiment, however, often drives the animals far from their normal biological circumstances and thus is difficult to interpret in terms of the undisturbed group dynamics. Here, we instead harness a natural biological response to a more typical environmental stimulus. We study mating swarms of the nonbiting midge *C. riparius*, which nucleate in the wild above ground-based visual features known as swarm markers (21, 22). These markers tend to localize swarms, although the motion of individual midges is highly convoluted (Fig. 1A). Previously, we showed that moving the swarm marker exerts an effective stress on the swarm and that quasi-statically separating two initially contiguous swarm markers can pull an existing swarm apart into two stable smaller swarms (18). We observed a mutual attraction of the two resulting subswarms when they were not too far apart, suggesting the existence of an effective elastic modulus for the swarm as a whole. However, since the effective stress applied to the swarms by the marker was unknown, we could not measure this modulus. Here, we go beyond these quasi-static measurements by oscillating the swarm marker (Fig. 1B) in analogy with dynamic mechanical spectroscopy experiments (23), circumventing the problem of the unknown stress and allowing us to extract group-level “material properties” of the swarm. Further details of our experiments are provided in the Materials and Methods section.

## Bulk swarm response

When we oscillate the swarm marker sinusoidally at moderate frequencies  $f$  and amplitudes  $A_M$ , we find that the swarm moves along with the marker. This effect is most apparent in  $X_S(t)$ , the time-dependent phase-averaged position of the swarm center of mass along the axis of oscillation (Fig. 1C). The swarm tracks the marker and moves at the same frequency, albeit with a smaller amplitude and a phase lag. By fitting this phase-averaged swarm response with a sinusoid, we can extract its amplitude  $A_S$ . This amplitude varies linearly with the amplitude of the marker oscillation  $A_M$  (Fig. 1D), allowing us to use linear response theory to characterize the driven swarm behavior (23).

<sup>1</sup>Department of Civil and Environmental Engineering, Stanford University, Stanford, CA 94305, USA. <sup>2</sup>Rothamsted Research, Harpenden, Hertfordshire AL5 2JQ, UK.

\*Corresponding author. Email: nto@stanford.edu

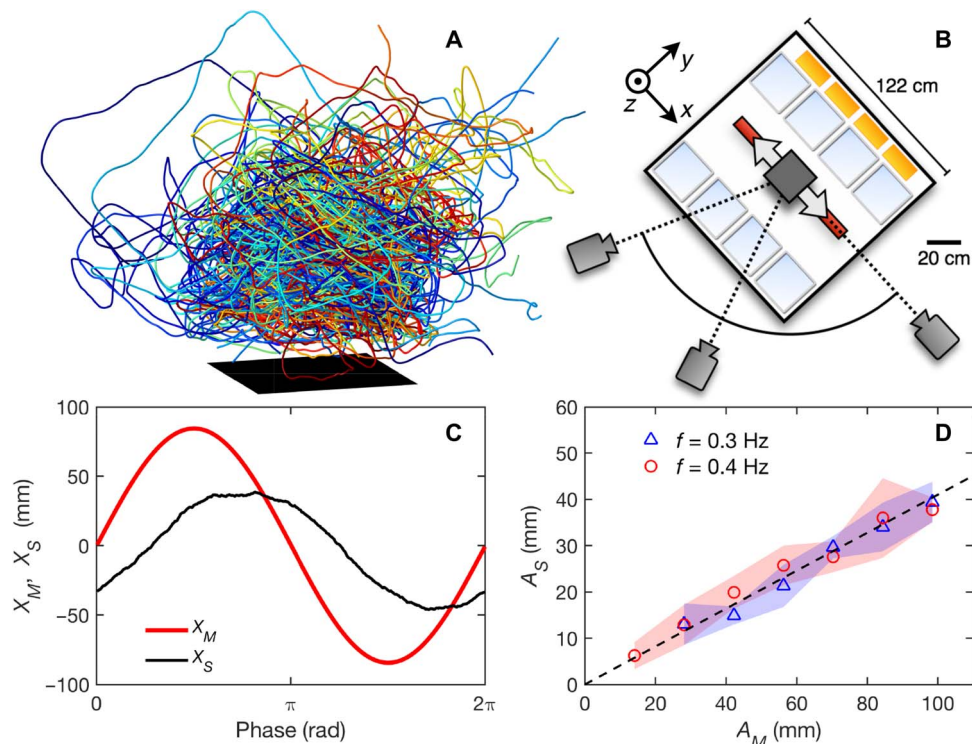


**Fig. 1. Mean swarm response to an oscillating swarm marker.** (A) Trajectories (>40 s long) of individual midges (each color corresponding to a different midge) are individually convoluted but remain localized over the ground-based swarm marker (black square). (B) Sketch of our experimental setup. Swarms form inside a plexiglass cube measuring 122 cm on a side and are imaged using three cameras mounted outside the enclosure. The swarm marker (in dark gray) is mounted on a linear stage (in red) that can be oscillated over a range of controlled frequencies and amplitudes along the direction indicated by the white arrows, which we label as the  $x$  direction.  $z$  increases vertically from the swarm marker (antiparallel to gravity), with the marker itself at  $z = 0$ . Midge development tanks (light blue) and four infrared light-emitting diode arrays (yellow; additional arrays on top of the enclosure are not shown) are also shown. (C) Phase-averaged position of the center of the swarm marker  $X_M$  and the center of mass of the swarm  $X_S$ . The swarm center of mass tracks the sinusoidal motion of the marker, although with a reduced amplitude and a phase lag. (D) The amplitude of the swarm center-of-mass motion  $A_S$  as a function of the amplitude of the marker motion  $A_M$  for two different oscillation frequencies, showing a linear relationship between the two. The shaded area shows the SEM.

### Vertical variation of the swarm response

Focusing only on the center of mass can hide the details of how the stimulus (that is, the movement of the marker) modulates the swarm. For example, information about external predators has been observed to propagate as a traveling wave through bird flocks rather than affecting all the birds at once (24). One might therefore expect that the response of the swarm ought to depend on the distance from the marker, since it is the source of the stimulus. To test this hypothesis, we looked at lateral slabs of the swarm, defined as volumes of the swarm that extend over the full range of the horizontal coordinates  $x$  and  $y$  in the swarm but only over a small range in the vertical coordinate  $z$  (see Materials and Methods), allowing us to retain aspects of the group-level response rather than considering only individuals. We studied the phase-averaged behavior of these slabs as a function of the vertical distance  $z$  away from the marker, where  $z = 0$  lies on the marker (Fig. 2A). Just as for the swarm as a whole, these slabs oscillate at the same angular frequency  $\omega$  as the marker and are well fit by sinusoidal functions of the form  $A_S(z) \sin(\omega t - \phi)$  (Fig. 2A); but the phase-averaged amplitude  $A_S(z)$  and the phase lag  $\phi(z)$  are functions of  $z$  (Fig. 2, B and C). For both the amplitude and phase, there is a region at the bottom of the swarm near the marker where the swarm response is rigid and almost independent of  $z$ . From roughly 1 of 3 of the total height of the swarm upward, however,  $A_S(z)$  decays and  $\phi$  increases with increasing  $z$  (Fig. 2, B and C). We attribute the finite

phase shift close to the marker to the nondirect coupling between the marker and the swarm (since the effective stress is not a contact stress) and treat it simply as a net phase difference experienced by the entire swarm.

Above the bottom rigid region, the behavior is suggestive of a damped traveling shear wave propagating through the swarm (Fig. 2D). Since, as noted above, the amplitude of the swarm response is linear in the driving amplitude, we assume that the swarm deformation is also linear in the (unknown) effective stress applied by the marker. Hence, we model the swarm as a general linear stress-strain material (23). We note that by treating the stimulation applied by the marker as a stress, we are implicitly making a continuum assumption for the swarms. Although this assumption is difficult to evaluate independently, since we do not know the relevant internal length scales in the swarm, it is reasonable given that the laterally averaged deformation of the swarm is smooth in  $z$  (Fig. 2D). We can then borrow insight from the medical imaging community, where shear waves are excited in tissue by direct contact or ultrasound and the wave characteristics are used to extract its material properties (25, 26). The time-dependent amplitude  $S$  of a damped shear wave propagating in the  $z$  direction can be written as

$$S(z, t) = S_0 e^{-k_z z} \cos(\omega t - k_r z) \quad (1)$$

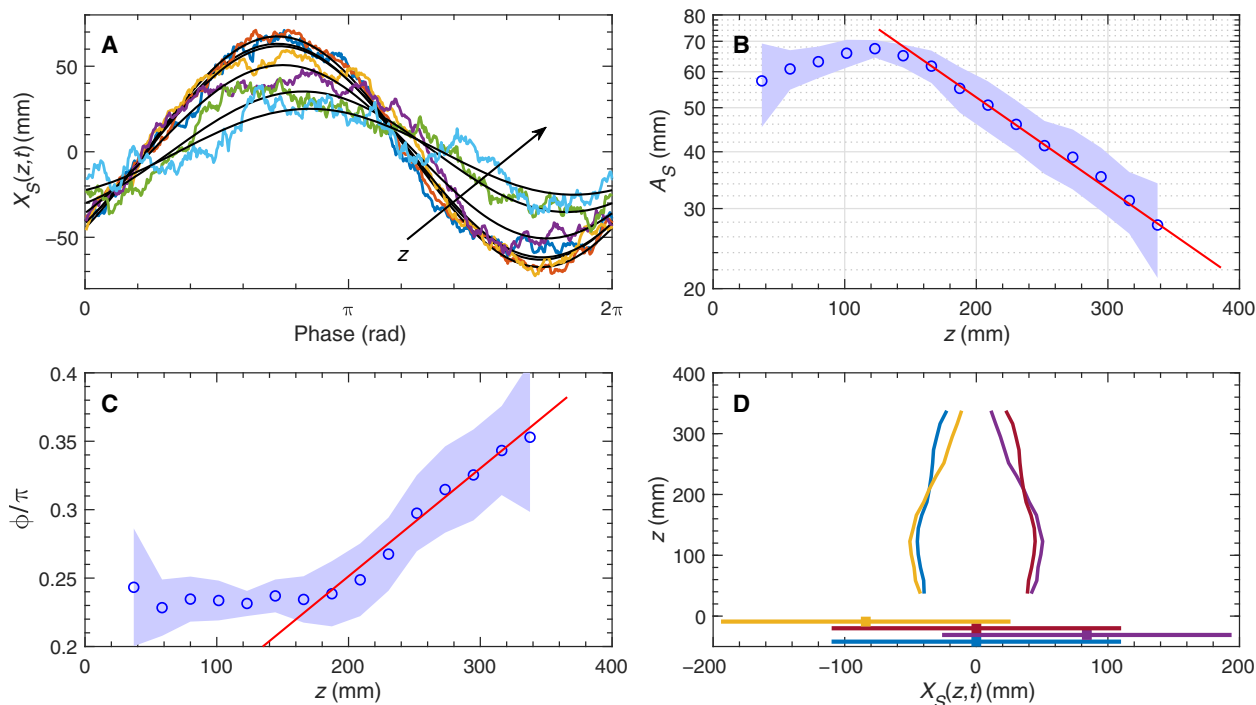


**Fig. 2. Height-dependent swarm response for a fixed amplitude of  $A_M = 84$  mm.** (A) Phase-averaged mean position of laterally averaged slabs of the swarm  $X_S(z,t)$  at different heights  $z$  above the marker. As  $z$  increases, the amplitude of the swarm motion decreases. Black solid lines are sinusoidal fits. For clarity, we only show the response for a subset of  $z$  values (80, 123, 166, 209, 295, and 338 mm). (B) The amplitude  $A_S(z)$  of  $X_S(z,t)$  as a function of  $z$ . The shaded area shows the 95% confidence interval, and the red line is an exponential fit. The vertical axis is logarithmic. (C) The phase lag  $\phi$  (in units of  $\pi$ ) between  $X_M$  and  $X_S(z,t)$  as a function of  $z$ . The red line is a linear fit. (D) Vertical profiles of  $X_S(z,t)$  at four fixed phases of the driving, revealing the shape of the traveling shear wave. Unlike in (A), where each  $X_S(z,t)$  curve has fixed  $z$  but variable  $t$ , here, each curve has fixed  $t$  but variable  $z$ . The horizontal colored lines at the bottom of the figure show the time-dependent position of the swarm marker corresponding to each of the profiles.

where  $S_0$  is an overall constant [so that  $A_S(z) = S_0 e^{-k_i z}$ ] and  $k_r$  and  $k_i$  are the real and imaginary parts, respectively, of a complex wavenumber  $k^*$ . This simple model predicts that  $A_S(z)$  should decay exponentially with  $z$  and that  $\phi$  should increase linearly with  $z$ . Both of these predictions are compatible with our measurements (Fig. 2, B and C).

### Effective material properties of midge swarms

Fitting the dependence of  $A_S(z)$  and  $\phi(z)$  on  $z$  allows us to determine  $k^*$ , which, in turn, allows us to extract the mechanical response properties of the swarms. In particular,  $k^*$  is related to the complex shear modulus  $G^* = G' + iG''$  by  $k^* = \sqrt{\rho\omega^2/G^*}$ , where  $\rho$  is the material density, which we estimate here as the product of the typical mass of a midge (approximately 2 mg) and the midge number density. For a viscoelastic material, the storage modulus  $G'$  (that is, the real part of  $G^*$ ) measures the elastic energy stored in the shear wave, while the loss modulus  $G''$  (that is, the imaginary part of  $G^*$ ) measures the energy that is dissipated as the wave propagates. Assuming a uniform  $\rho$ , we find that both  $G'$  and  $G''$  are nonzero (Fig. 3, A and B) so that the swarms respond as if they are fully viscoelastic.  $G'$  is negative and varies quadratically with frequency, suggesting that the behavioral response of midges to the motion of conspecifics endows the swarms with an effective inertia (26). A negative  $G'$  also implies both a long wavelength and a rapid attenuation, meaning that the swarm as a whole strongly damps the shear wave. We can also measure the dispersion relation for the shear-wave speed (Fig. 3C), which increases linearly with the driving frequency and is of the same order of magnitude as typical midge velocities (27).

To relate the storage and loss moduli to static material properties such as elasticity  $G_0$  and viscosity  $\eta$ , a constitutive law is needed. Standard models of linear viscoelastic materials that characterize material response via a combination of purely elastic and purely viscous elements, however, cannot reproduce the negative storage modulus we observe (23). By adding an additional effective inertial mass, however, we can capture this behavior (26). In particular, if we model the swarm response as an elastic element and a viscous element connected in parallel (a Kelvin-Voigt model), with an additional inertial mass connected in series, then we would expect to find  $G' = G_0 - \omega^2 G_M$  and  $G'' = \omega\eta$ , where  $G_M$  is a measure of the effective inertia of the swarm (26). These forms fit our data very well (Fig. 3, A and B), suggesting that this simple mass-spring-damper model accurately captures the emergent mechanical properties of the swarms. The elasticity of the swarm can be seen as a manifestation of its internal cohesion and the viscosity as its resistance to flow.

For our swarms, we find  $G_0 = 1.7 \pm 7 \mu\text{Pa}$ ,  $\eta = 35.8 \pm 0.2 \mu\text{Pa s}$ , and  $G_M = 29.5 \pm 0.2 \text{ mg/mm}$ . The ratio  $G''/G_0$  is a measure of the degree of damping in a material (23), with the inertial contribution removed (26). For our swarms, this ratio ranges from 3 to 62, showing that they are strongly damping.

### Stochastic modeling

Our experimental results suggest that swarms have an effective viscoelastic modulus that emerges from interactions between the individuals, with midges high in the swarm responding the motion of those just below them rather than independently to the movement of the marker

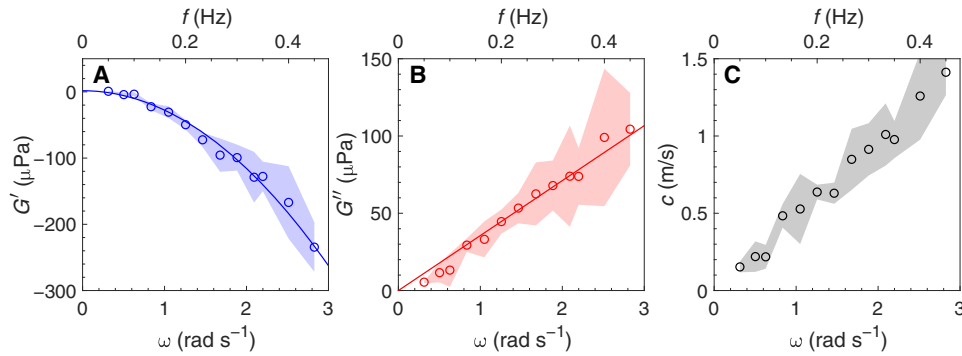


**Fig. 3. Swarm material properties.** (A) Storage modulus  $G'$  as a function of driving frequency, reported for both angular frequency (bottom axis) and linear frequency (top axis), for a fixed amplitude of  $A_M = 84$  mm. The solid line is a parabolic fit. (B) Loss modulus  $G''$  as a function of frequency for the same data as in (A). The solid line is a linear fit. (C) Dispersion relation relating the shear wave speed  $c$  and the driving frequency. For all panels, the shaded areas show the SEM and are the result of averaging over different swarming events.

itself. However, there is a possibility that the effects we observe may arise from this individual visual processing when combined with parallax and possible optomotor response (28). In this case, the viscoelasticity we see would be the result of the particular visual stimulus and not a generic property of the swarms.

To address this question, we turned to the stochastic swarm model of Reynolds *et al.* (29), which has been shown to reproduce a plethora of recent observations for midge swarms (30). For our purposes, this model makes no assumptions about the specific nature of the sensory systems of the midges, and so perturbing the model swarms is agnostic as to the physical nature of the perturbation. Midges in this model are treated as simple self-propelled point particles. Interactions between the individuals are not explicitly described; rather, their net effect is subsumed into a harmonic restoring force, since experimental observations have suggested that to leading order midges appear to be tightly bound to the swarm itself but weakly coupled to each other inside it (31).

In the model, the positions  $\mathbf{x}$  and velocities  $\mathbf{u}$  of midges are given by the solutions of the stochastic differential equations

$$\begin{aligned} du_i &= -\frac{u_i}{T} dt + \langle A_i | u, x \rangle dt + \sqrt{\frac{2\sigma_u^2}{T}} dW_i(t) \\ dx_i &= u_i dt \end{aligned} \quad (2)$$

where the subscripts denote Cartesian components,  $T$  is a velocity autocorrelation timescale,  $\sigma_u$  is the root-mean-square speed, and  $dW(t)$  is an incremental Wiener process with correlation property  $dW_i(t)dW_j(t + \tau) = \delta(\tau)\delta_{ij}dt$ . Although all three Cartesian directions in the model are a priori equivalent, we label the  $x_3$  direction as  $z$  in analogy with the experiments; note that the point  $z = 0$  lies at the center of mass of the swarm. The first term is a memory term that causes velocity fluctuations to relax back to their (zero) mean value. The second term, the mean conditional acceleration that expresses the effective restoring force that binds individuals to the swarm, is given in spherical coordinates by

$$\begin{aligned} \langle A_1 | u, x \rangle &= \cos(\hat{\theta})\sin(\hat{\phi})A_s \\ \langle A_2 | u, x \rangle &= \sin(\hat{\theta})\sin(\hat{\phi})A_s \\ \langle A_3 | u, x \rangle &= \cos(\hat{\phi})A_s \\ A_s &= -3r \frac{\sigma_u^2}{\sigma_r^2} [\sin \hat{\phi} \sin \phi \cos(\hat{\theta} - \theta) + \cos \hat{\phi} \cos \phi] \end{aligned} \quad (3)$$

where  $r$  is the radial distance from the swarm center,  $\theta$  and  $\phi$  are the polar and azimuthal angles of the position vector,  $\hat{\theta}$  and  $\hat{\phi}$  are the polar and azimuthal angles of the velocity vector,  $\sigma_r$  is the root-mean-square size of the swarm,  $x_1 = r \cos \theta \sin \phi$ ,  $x_2 = r \sin \theta \sin \phi$ ,  $x_3 = r \cos \phi$ ,  $u_1 = s \cos \hat{\theta} \sin \hat{\phi}$ ,  $u_2 = s \sin \hat{\theta} \sin \hat{\phi}$ ,  $u_3 = s \cos \hat{\phi}$ , and  $s$  is the midge's flight speed. The third term is the stochastic driving noise. Equation 2 is effectively a first-order autoregressive stochastic process in which position and velocity are assumed to be jointly Markovian. By construction, simulated trajectories are consistent with spherically symmetric swarms with Gaussian density profiles and homogeneous (position independent) Gaussian velocity statistics. The model contains three free parameters ( $\sigma_r$ ,  $\sigma_u$ , and  $T$ ); here, we set them all to unity as we are primarily interested in qualitative rather than quantitative comparisons.

To test the response of the simulated swarms to perturbations in a way that does not presuppose a particular behavioral coupling, we simply force the horizontal position of the swarm center  $\bar{x}$  to oscillate along the  $x_1$  axis. Physically, this corresponds to assuming that the stimulus acts on individuals only via the effective emergent properties of the swarm rather than directly. We find that, just as in the experiments, this stimulus propagates away from the center of the modeled swarm in a way that is consistent with wave motion (Fig. 4). For both the amplitude  $A_S(z)$  and the phase  $\phi(z)$ , computed in the same way as in the experiments, there is a region close to the stimulus where the swarm response is rigid and almost independent of  $z$ , the vertical distance to the center of mass. Above this region,  $A_S(z)$  decreases exponentially with height, while  $\phi(z)$  increases linearly with height—just as observed for the real midges. Taking the modeling one step further, we can use the wave amplitude and phase to compute a shear modulus as we did above. Again, in agreement with the experimental observations, the simulated swarms have a storage modulus  $G'$  that is negative at sufficiently high frequencies and scales quadratically with frequency (Fig. 5A), indicating an effective inertial mass, and a loss modulus  $G''$  that increases monotonically with frequency (Fig. 5B). Thus, this simple low-order swarm model reproduces the mechanical properties observed in the experimental swarms while not assuming any response that is particular to the midge visual system.

### DISCUSSION

Our results demonstrate that midge swarms respond to external stimuli so that the swarm as a whole functions as an actively damped material, with both viscous and inertial contributions. Viscoelasticity has been



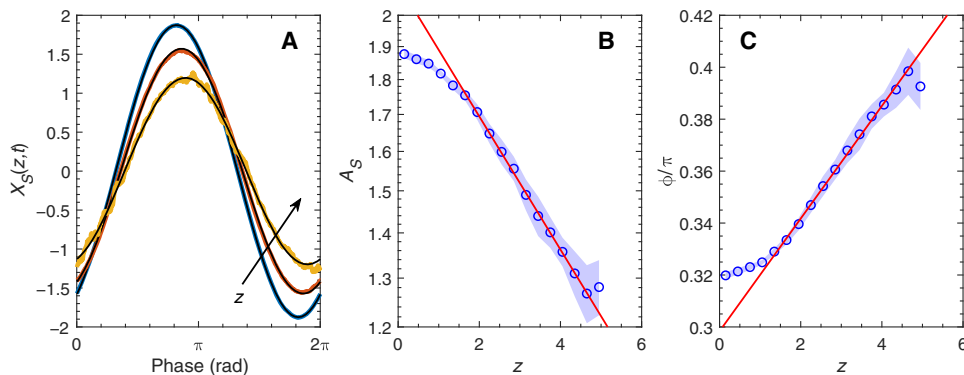


**Fig. 4. Response of a swarm model.** (A) Phase-averaged mean position of laterally averaged slabs of the swarm model  $X_S(z,t)$  at different vertical distances  $z$  from the swarm center, where the oscillating perturbation is applied along  $x$ . As  $z$  increases, the amplitude of the swarm motion decreases. Black solid lines are sinusoidal fits. The amplitude of the oscillation of the center of attraction is 2, and the frequency of oscillation is  $0.65 \text{ rad s}^{-1}$ . (B) The amplitude  $A_S(z)$  of  $X_S(z,t)$  as a function of  $z$ . The shaded area shows the 95% confidence interval. The red line is an exponential fit. The vertical axis is logarithmic. (C) The phase lag  $\phi$  (in units of  $\pi$ ) between the oscillation of the swarm center and  $X_S(z,t)$  as a function of  $z$ . The shaded area shows the 95% confidence interval, and the red line is a linear fit. Results are shown for the case where all model parameters ( $\sigma_r$ ,  $\sigma_w$ , and  $T$ ) are set to unity in arbitrary units.

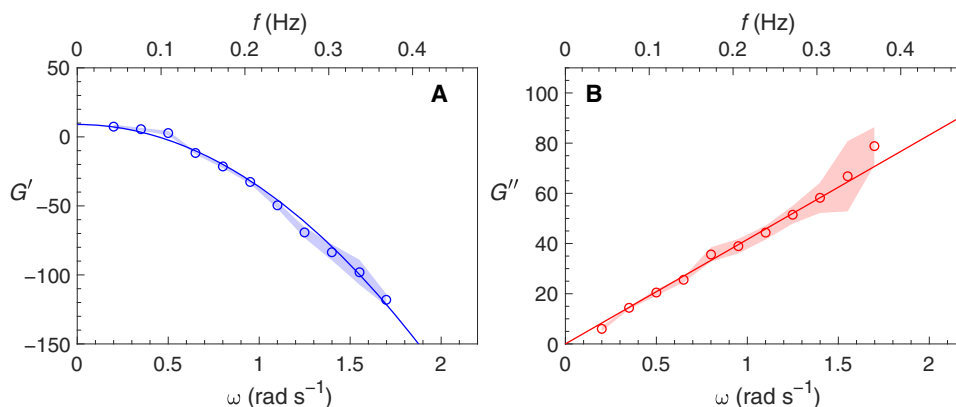


**Fig. 5. Model swarm material properties.** (A) Storage modulus  $G'$  of the swarm model as a function of driving frequency, reported for both angular frequency (bottom axis) and linear frequency (top axis), for a fixed amplitude of 2 and swarm density of 1. The solid line is a parabolic fit. (B) Loss modulus  $G''$  as a function of frequency for the same data as in (A). The solid line is a linear fit. For all panels, the shaded areas show the SEM. Results are shown for the case where all model parameters ( $\sigma_r$ ,  $\sigma_w$ , and  $T$ ) are set to unity in arbitrary units.

frequently reported in other active systems such as actin networks (32, 33). However, the situation here is different since there are no contact interactions between the midges. A midge swarm thus cannot support an actual mechanical load, in contrast to, for example, aggregations of ants that interlock their legs and transmit true mechanical stresses throughout the group (16). The effective viscoelasticity we observe here cannot be explained by typical active mechanics. Instead, it must emerge from the behavior of the individuals and is better interpreted as expressing a transfer of information through the swarm.

This behavioral response could come in two different forms: an independent response of each individual midge to the moving swarm marker or a collective response of the swarm where the information about the moving marker propagates through the swarm via interactions between the midges. Although we cannot fully rule out some degree of independent response, our measurements strongly suggest that the collective response is dominant. Simple geometric parallax, for example, would also predict a falloff of the response amplitude with height away from the marker, since the motion of the marker appears smaller for midges higher up in the swarm. However, an explanation in terms of parallax alone with no additional behavioral

response would not predict the systematic shift of the phase lag with height that we observe. Instead, this observation, when paired with the effective rigidity of the lowest layers of the swarm, suggests a scenario whereby midges at the bottom of the swarm directly perceive the marker and follow it, while midges higher in the swarm follow the motion of the midges below them instead of the marker itself. This scenario is compatible with our stochastic modeling results, where we found that an oscillation of the emergent potential that captures the collective behavior of the swarm led to the same kind of decaying shear waves as we saw in the experiment. Furthermore, in our previous studies, when we perturbed these swarms with acoustic signals (17), we argued that the response was not collective because there was no phase lag between any individuals—rather, all the midges phase-locked to the driving signal. What we see here is exactly the opposite. Thus, together, we interpret our results as indicative of an emergent, collective response of the swarm as a whole. We note that such an interpretation also implies that the stimulus we are applying to the swarm indeed allows us to measure an intrinsic property of the swarm, that is, its inherent emergent viscoelasticity, rather than changing the nature of the swarm.

When coupled with the strongly damping nature of the effective shear modulus, we are led to the conclusion that collective behavior in midge swarms functions to suppress imposed perturbations very efficiently and keeps the swarm stable and stationary even in a noisy, stochastic environment, in contrast to bird flocks where collective behavior has the opposite effect and promotes the lossless flow of information (34). These disparate results are consistent with the biological functions of these two types of aggregations. Male midges swarm to provide a mating target for females (21) so that stationarity is desirable, while birds and fish move together in part to enhance their collective safety against predator attack so that rapid information transfer is beneficial (24). Our findings thus demonstrate that these biological functions are reflected in the physical emergent properties of the aggregations and lend further support to the value of continuum descriptions of collective systems (35).

## MATERIALS AND METHODS

### Midge colony

We maintained a colony of *C. riparius* midges in a transparent cubical enclosure measuring 122 cm on a side (Fig. 1B). The midge enclosure was illuminated on a timed circadian cycle with 16 hours of light and 8 hours of darkness per day. *C. riparius* larvae developed in eight 10-liter tanks filled with dechlorinated tap water and outfitted with bubbling air supplies to ensure that the water is sufficiently oxygenated. We provided a cellulose substrate into which the larvae can burrow. The water was cleaned twice a week; after cleaning, the midge larvae were fed crushed, commercially purchased rabbit food. During their time in the breeding tanks, midge larvae transformed into pupae, and in the last few days of their life cycle, the pupae hatched and adult flying midges emerged out of the water.

### Experiments

Male *C. riparius* midges swarm spontaneously at dusk as part of their mating ritual. To position the swarms in the field of view of our cameras, we used a black square plate as a “swarm marker” (21); swarms nucleate above this marker. Swarms typically have a spheroidal shape that does not vary much from swarm to swarm, and the spatial size of the swarms is set dynamically by the midges based on the number of individuals participating (27). The swarm marker was attached to a linear stage with a position accuracy of 14  $\mu\text{m}$  (CS Series Belt Drive with NEMA 23 Brushless Servo Motor, Newmark Systems) that moves the swarm marker in a sinusoidal fashion with angular frequency  $\omega = 2\pi f$  (where  $f$  is the linear frequency), amplitude  $A_M$ , and maximum speed  $v = \omega A_M$ . The period of oscillation of the marker is  $T = 1/f$ . The stage was hardware synchronized to the imaging equipment. The operating noise of the linear stage does not disturb the midges, since it is quieter than the ambient noise due to the air supplies for the breeding tanks.

The experimental protocol was as follows. A recording session would start 30 min before the onset of swarming with calibration of the cameras (see “Imaging and identification” section). After the onset of swarming, we waited until the swarm grew to roughly 20 individuals and then started the marker movement. The swarm would be startled by the sudden movement of the marker so we waited roughly 1 min until starting to record images. Multiple separate recordings would be done in such a session, with varying oscillation amplitude and/or frequency of the marker. A recording session is finished when the swarm size fell below 20 individuals.

### Imaging and identification

We film the swarms with three hardware-synchronized cameras (Point Grey Flea3 1.3 MP Mono USB3 Vision) at 100 frames/s. The midges were illuminated in the near infrared using 20 light-emitting diode arrays that draw roughly 3 W of power each, four of which were placed inside the enclosure with the remaining arrays positioned on top of the enclosure. Because infrared light is invisible to the midges, it does not disturb their natural behavior, but is detectable by our cameras. The three cameras were arranged in a horizontal plane on three tripods, with angular separations of approximately 30° and 70° (Fig. 1B). To calibrate the imaging system, we assumed a standard pinhole camera model (36). The camera parameters were determined by fits to images of a calibration target consisting of a regular dot pattern. The calibration target was removed before swarming begins. Between 30,000 and 100,000 frames of data were recorded for each experiment, depending on the driving frequency of the marker; for experiments at lower frequencies, more frames were acquired to record sufficient full periods of oscillation. We performed a total of 29 experiments at varying amplitude and fixed frequencies of  $f = 0.3$  and 0.4 Hz and 20 experiments at constant amplitude  $A_M = 84$  mm and varying frequency. In the 49 swarms we recorded, the number of midges ranged from 20 to 70 individuals. To identify individual midges in the swarm, we first located the midges on each two-dimensional (2D) camera frame by finding the centroids of regions that had sufficient contrast with the background after subtraction of the average background and were larger than an appropriate threshold size. When possible, we split larger non-symmetrical regions that consisted of the images of two midges. After identification, the 2D locations determined from each camera were stereo-matched by projecting their coordinates along a line in 3D space using the calibrated camera models and looking for (near) intersections (36). For the results presented here, we have conservatively considered only midges that were seen unambiguously by all three cameras. Although in principle, two views are sufficient for stereo-imaging, in practice, at least three cameras were typically required to resolve ambiguities and avoid ghost midges. Arranging all three cameras in a plane, as we have done here, can still leave some residual ambiguity; this situation, however, occurs extremely infrequently and is more than compensated for by the simpler and superior camera calibration that can be obtained when all the cameras are positioned orthogonally to the walls of the midge enclosure. After identifying the 3D positions of the midges at every time step, we reconstructed their trajectories using a multiframe predictive particle tracking algorithm (37, 38).

### Data analysis

The time-dependent position of the center of mass  $\bar{x}(t)$  of the swarm is calculated as

$$\bar{x}(t) = \frac{1}{N(t)} \sum_{j=1}^{N(t)} x_j(t)$$

where  $x_j(t)$  is the 1D position (along the axis of oscillation of the marker) of midge  $j$  at time  $t$  and  $N(t)$  is the number of individuals in the swarm at time  $t$ . We calculated the phase-averaged position of the center of mass  $X_S(t)$  by averaging  $\bar{x}(t)$  over the period of oscillation of the marker  $T$  via

$$X_S(t) = \frac{1}{M} \sum_{i=0}^{M-1} \bar{x}(t + iT), \quad (0 < t < T)$$

where  $M$  is the duration of the experiment in full periods  $T$ . When computing the phase-averaged position of the center of mass as a function of height  $X_S(z, t)$ , we binned individuals in 40-mm tall horizontal slabs, spaced 20 mm apart. We fit  $X_S(t)$  and  $X_S(z, t)$  using functions of the form  $A_S \sin(\omega t - \phi)$  to obtain  $A_S$  and  $A_S(z)$ , the average and height-dependent amplitude of oscillation of the swarm, respectively, as well as  $\phi$  and  $\phi(z)$ , the average and height-dependent phase of the swarm, respectively. Subsequently, we fit  $A_S(z)$  and  $\phi(z)/\pi$  with functions of the form  $S_0 e^{-k_r z}$  and  $k_r z/\pi$ , respectively, to obtain values for  $k_r$  and  $k_i$ . The viscoelastic moduli  $G'$  and  $G''$  can be expressed in terms of  $k_r$  and  $k_i$  as

$$G' = \rho \omega^2 \frac{k_r^2 - k_i^2}{(k_r^2 + k_i^2)^2}$$

and

$$G'' = \rho \omega^2 \frac{2k_r k_i}{(k_r^2 + k_i^2)^2}$$

obtained by solving  $k_r - ik_i = \sqrt{\rho \omega^2 / (G' + iG'' )}$ .

We approximate the average swarm mass density  $\rho$  for each measurement by calculating the average number density in a sphere of 100 mm radius centered at the instantaneous center of mass of the swarm (to avoid edge effects) and subsequently multiplying this average with the typical midge weight of  $2.3 \pm 0.2$  mg. The swarm density varies by up to 30% between experiments, and while  $G'$  and  $G''$  are independent of  $\rho$ , the wave speed is not. The SD in  $G'$  and  $G''$  measured from different swarms is roughly 15%.

## REFERENCES AND NOTES

- J. K. Parrish, L. Edelstein-Keshet, Complexity, pattern, and evolutionary trade-offs in animal aggregation. *Science* **284**, 99–101 (1999).
- D. J. T. Sumpter, The principles of collective animal behaviour. *Philos. Trans. R. Soc. Lond B Biol. Sci.* **361**, 5–22 (2006).
- A. Cavagna, I. Giardina, Bird flocks as condensed matter. *Annu. Rev. Condens. Matter Phys.* **5**, 183–207 (2014).
- A. Berdahl, C. J. Torney, C. C. Ioannou, J. J. Faria, I. D. Couzin, Emergent sensing of complex environments by mobile animal groups. *Science* **339**, 574–576 (2013).
- N. J. Mot, C. A. Tovey, D. L. Hu, Fire ants self-assemble into waterproof rafts to survive floods. *Proc. Natl. Acad. Sci. U.S.A.* **108**, 7669–7673 (2011).
- S. J. Portugal, T. Y. Hubel, J. Fritz, S. Heese, D. Trobe, B. Voelkl, S. Hales, A. M. Wilson, J. R. Usherwood, Upwash exploitation and downwash avoidance by flap phasing in ibis formation flight. *Nature* **505**, 399–402 (2014).
- D. M. Gordon, The rewards of restraint in the collective regulation of foraging by harvester ant colonies. *Nature* **498**, 91–93 (2013).
- J. Korb, Thermoregulation and ventilation of termite mounds. *Naturwissenschaften* **90**, 212–219 (2003).
- S. A. Ocko, H. King, D. Andreen, P. Bardunias, J. S. Turner, R. Soar, L. Mahadevan, Solar-powered ventilation of African termite mounds. *J. Exp. Biol.* **220**, 3260–3269 (2017).
- J. Krause, G. D. Ruxton, S. Krause, Swarm intelligence in animals and humans. *Trends Ecol. Evol.* **25**, 28–34 (2009).
- E. Bonabeau, M. Dorigo, G. Theraulaz, Inspiration for optimization from social insect behaviour. *Nature* **406**, 39–42 (2000).
- J. Werfel, K. Petersen, R. Nagpal, Designing collective behavior in a termite-inspired robot construction team. *Science* **343**, 754–758 (2014).
- T. Vicsek, A. Czirók, E. Ben-Jacob, I. Cohen, O. Shochet, Novel type of phase transition in a system of self-driven particles. *Phys. Rev. Lett.* **75**, 1226–1229 (1995).
- W. Bialek, A. Cavagna, I. Giardina, T. Mora, E. Silvestri, M. Viale, A. M. Walczak, Statistical mechanics for natural flocks of birds. *Proc. Natl. Acad. Sci. U.S.A.* **109**, 4786–4791 (2012).
- R. Lukeman, Y.-X. Li, L. Edelstein-Keshet, Inferring individual rules from collective behavior. *Proc. Natl. Acad. Sci. U.S.A.* **107**, 12576–12580 (2010).
- M. Tennenbaum, Z. Liu, D. Hu, A. Fernandez-Nieves, Mechanics of fire ant aggregations. *Nat. Mater.* **15**, 54–59 (2015).
- R. Ni, J. G. Puckett, E. R. Dufresne, N. T. Ouellette, Intrinsic fluctuations and driven response of insect swarms. *Phys. Rev. Lett.* **115**, 118104 (2015).
- R. Ni, N. T. Ouellette, On the tensile strength of insect swarms. *Phys. Biol.* **13**, 045002 (2016).
- M. Sinhuber, N. T. Ouellette, Phase coexistence in insect swarms. *Phys. Rev. Lett.* **119**, 178003 (2017).
- D. T. Swain, I. D. Couzin, N. E. Leonard, Real-time feedback-controlled robotic fish for behavioral experiments with fish schools. *Proc. IEEE* **100**, 150–163 (2011).
- A. E. R. Downe, V. G. Caspary, The swarming behaviour of *Chironomus riparius* (Diptera: Chironomidae) in the laboratory. *Can. Entomol.* **105**, 165–171 (1973).
- J. G. Puckett, N. T. Ouellette, Determining asymptotically large population sizes in insect swarms. *J. R. Soc. Interface* **11**, 20140710 (2014).
- K. P. Menard, *Dynamic Mechanical Analysis: A Practical Introduction* (CRC Press, 2008).
- A. Procaccini, A. Orlandi, A. Cavagna, I. Giardina, F. Zoratto, D. Santucci, F. Chiarotti, C. K. Hemelrijk, E. Alleva, G. Parisi, C. Carere, Propagating waves in starling, *Sturnus vulgaris*, flocks under predation. *Anim. Behav.* **82**, 759–765 (2011).
- G.-Y. Li, Y. Cao, Mechanics of ultrasound elastography. *Proc. R. Soc. A* **473**, 20160841 (2017).
- X. Yang, C. C. Church, A simple viscoelastic model for soft tissues—the frequency range 6–20 MHz. *IEEE Trans. Ultrason. Ferroelectr. Freq. Control* **53**, 1404–1411 (2006).
- D. H. Kelley, N. T. Ouellette, Emergent dynamics of laboratory insect swarms. *Sci. Rep.* **3**, 1073 (2013).
- A. Borst, J. Haag, D. F. Reiff, Fly motion vision. *Annu. Rev. Neurosci.* **33**, 49–70 (2010).
- A. M. Reynolds, M. Sinhuber, N. T. Ouellette, Are midge swarms bound together by an effective velocity-dependent gravity? *Eur. Phys. J. E* **40**, 46 (2017).
- A. M. Reynolds, Langevin dynamics encapsulate the microscopic and emergent macroscopic properties of midge swarms. *J. R. Soc. Interface* **15**, 20170806 (2018).
- J. G. Puckett, D. H. Kelley, N. T. Ouellette, Searching for effective forces in laboratory insect swarms. *Sci. Rep.* **4**, 4766 (2014).
- W. W. Ahmed, E. Fodor, T. Betz, Active cell mechanics: Measurement and theory. *Biochim. Biophys. Acta* **1853**, 3083–3094 (2015).
- A. R. Bausch, W. Möller, E. Sackmann, Measurement of local viscoelasticity and forces in living cells by magnetic tweezers. *Biophys. J.* **76**, 573–579 (1999).
- A. Attanasi, A. Cavagna, L. Del Castello, I. Giardina, T. S. Grigera, A. Jelić, S. Melillo, L. Parisi, O. Pohl, E. Shen, M. Viale, Information transfer and behavioural inertia in starling flocks. *Nat. Phys.* **10**, 691–696 (2014).
- N. Bain, D. Bartolo, Dynamic response and hydrodynamics of polarized crowds. *Science* **363**, 46–49 (2019).
- R. Y. Tsai, A versatile camera calibration technique for high-accuracy 3D machine vision metrology using off-the-shelf TV cameras and lenses. *IEEE J. Rob. Autom.* **3**, 323–344 (1987).
- N. T. Ouellette, H. Xu, E. Bodenschatz, A quantitative study of three-dimensional Lagrangian particle tracking algorithms. *Exp. Fluids* **40**, 301–313 (2006).
- D. H. Kelley, N. T. Ouellette, Using particle tracking to measure flow instabilities in an undergraduate laboratory experiment. *Am. J. Phys.* **79**, 267–273 (2011).

**Acknowledgments:** We thank R.H. Ewoldt and A. Borst for helpful discussions. **Funding:** This research was sponsored by the Army Research Laboratory and accomplished under grant no. W91NF-16-1-0185. The views and conclusions in this document are those of the authors and should not be interpreted as representing the official policies, either expressed or implied, of the Army Research Laboratory or the U.S. government. K.v.d.V. acknowledges support from an Early Postdoc Mobility fellowship from the Swiss National Science Foundation. M.S. acknowledges support from the Deutsche Forschungsgemeinschaft under grant no. 396632606. The work at Rothamsted forms part of the Smart Crop Protection (SCP) strategic programme (BBS/OS/CP/000001) funded through Biotechnology and Biological Sciences Research Council's Industrial Strategy Challenge Fund. **Author contributions:** K.v.d.V. and N.T.O. designed the research, K.v.d.V. and M.S. conducted the experiments. K.v.d.V. analyzed the data. A.M.R. developed and ran the stochastic model. All authors interpreted the data and wrote the paper. **Competing interests:** The authors declare that they have no competing interests. **Data and materials availability:** All data needed to evaluate the conclusions in the paper are present in the paper. Additional data related to this paper may be requested from the authors.

Submitted 6 February 2019

Accepted 3 June 2019

Published 10 July 2019

10.1126/sciadv.aaw9305

**Citation:** K. van der Vaart, M. Sinhuber, A. M. Reynolds, N. T. Ouellette, Mechanical spectroscopy of insect swarms. *Sci. Adv.* **5**, eaaw9305 (2019).



## Mechanical spectroscopy of insect swarms

Kasper van der Vaart, Michael Sinhuber, Andrew M. Reynolds and Nicholas T. Ouellette

*Sci Adv* **5** (7), eaaw9305.  
DOI: 10.1126/sciadv.aaw9305

**ARTICLE TOOLS** <http://advances.sciencemag.org/content/5/7/eaaw9305>

**REFERENCES** This article cites 37 articles, 8 of which you can access for free  
<http://advances.sciencemag.org/content/5/7/eaaw9305#BIBL>

**PERMISSIONS** <http://www.sciencemag.org/help/reprints-and-permissions>

Use of this article is subject to the [Terms of Service](#)

---

*Science Advances* (ISSN 2375-2548) is published by the American Association for the Advancement of Science, 1200 New York Avenue NW, Washington, DC 20005. 2017 © The Authors, some rights reserved; exclusive licensee American Association for the Advancement of Science. No claim to original U.S. Government Works. The title *Science Advances* is a registered trademark of AAAS.